JCTC Journal of Chemical Theory and Computation

Article

pubs.acs.org/JCTC

Quantum Mechanical Study of Vicinal J Spin−Spin Coupling Constants for the Protein Backbone

Bing Wang,[†] Xiao He,*[,‡] and Kenneth M. Merz*[,†]

[†]Department of Chemistry and the Quantum Theory Project, University of Florida, Gainesville, Florida, 32611, United States

[‡]State Key Laboratory of Precision Spectroscopy and Department of Physics, Institute of Theoretical and Computational Science, East China Normal University, Shanghai 200062, China

Supporting Information

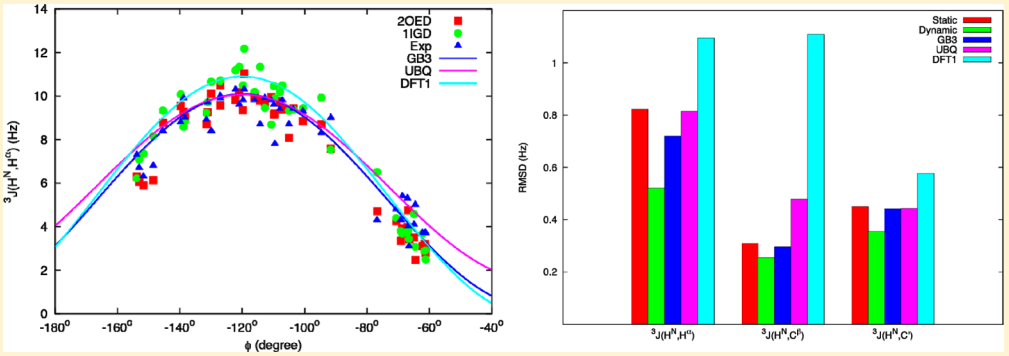

ABSTRACT: We have performed density functional theory (DFT) calculations of vicinal J coupling constants involving the backbone torsional angle for the protein GB3 using our recently developed automatic fragmentation quantum mechanics/molecular mechanics (AF-QM/MM) approach (Xiao He et al. *J. Phys. Chem. B* **2009**, *113*, 10380−10388). Interestingly, the calculated values based on an NMR structure are more accurate than those based on a high-resolution X-ray strucure because the NMR structure was refined using a large number of residual dipolar couplings (RDCs) whereas the hydrogen atoms were added into the X-ray structure in idealized positions, confirming that the postioning of the hydrogen atoms relative to the backbone atoms is important to the accuracy of J coupling constant prediction. By comparing three Karplus equations, our results have demonstrated that hydrogen bonding, substituent and electrostatic effects could have significant impacts on vicinal J couplings even though they depend mostly on the intervening dihedral angles. The root-mean-square deviations (RMSDs) of the calculated $^3J(H^N,H^\alpha)$, $^3J(H^N,C^\beta)$, $^3J(H^N,C')$ values based on the NMR structure are 0.52, 0.25, and 0.35 Hz, respectively, after taking the dynamic effect into consideration. The excellent accuracy demonstrates that our AF-QM/MM approach is a useful tool to study the relationship between J coupling constants and the structure and dynamics of proteins.

INTRODUCTION

It has long been recognized that three-bond (vicinal) nuclear spin−spin coupling constants are valuable resources for protein structure and dynamics. The most extensively studied vicinal coupling constants are those involving the backbone ϕ torsion angle: $^3J(H^N,H^\alpha)$, $^3J(H^N,C^\beta)$, $^3J(H^N,C')$, $^3J(C',H^\alpha)$, $^3J(C',C^\beta)$, and $^3J(C',C')$. The connection between those vicinal J-couplings and ϕ dihedral angle has been established by the empirical Karplus equation:[1,2]

$$^3J = A\cos^2(\phi + \theta) + B\cos(\phi + \theta) + C \quad (1)$$

where θ is the offset angle between angle and the dihedral angle directly relating to two measured spins. Parameters A, B, and C are usually determined by best-fitting observed J-couplings with the corresponding dihedral angles derived from high-resolution X-ray crystallographic structures.[3−9] Because a variety of experimental techniques have been developed for the accurate measurement of J-couplings over the years, several sets of Karplus parameters have been reported for small proteins in the literatures.[10−13] Karplus equation builds a direct bridge between experimental J-couplings and protein backbone structure and have been widely used in NMR structure determination and dynamical analysis of proteins.[14] A recent application of the Karplus equation was the validation of peptide conformational distributions generated by force fields used in molecular dynamics (MD) simulation.[15−17]

Despite its success, there are several concerns about the empirical Karplus relationship for protein structure and dynamics studies: (1) Karplus parameters are assumed to be independent of residue type and the surrounding environment. Consequently, side-chain specific substituent effects, hydrogen bonding, and electrostatic effects, which could have significant contributions to the J-coupling values,[18,19] are ignored or

Received: July 19, 2013
Published: August 22, 2013

simply averaged out. (2) $^3J(H^N,H^\alpha)$, $^3J(H^N,C^\beta)$, $^3J(H^N,C')$, and $^3J(C',H^\alpha)$ are not related directly to the ϕ angle $C'-N-C^\alpha-C'$ but to the dihedral angles involving the two corresponding nuclei. Hydrogen atoms are usually added to X-ray structures under the assumption of ideal planar peptide bonds during the parametrization of the Kaplus equation. However, it has been demonstrated that the amide moiety can be partially pyramidalized in peptide and protein structures, causing the amide proton to bend out of the peptide plane.[12,20,21] Such deviation from planarity of the amide group would cause uncertainties in the associated Karplus curves, as has been discussed by Bax and co-workers.[19] (3) The measured coupling constants represent the population-weighted averages of the instantaneous couplings over a time scale of milliseconds. The Karplus equation absorbs this dynamic effect in an average manner through the parametrization. Consequently, it is challenging to extract reliable dynamics information directly from the Karplus eqution. (4) The Karplus parameters are usually derived from a set of J coupling constants taken from one structure. Their transferability to other systems with less well characterized or unknown structures is still a subject for debate.

Recent advances in quantum chemistry, especially density functional theory (DFT), make it possible to calculate J coupling constants accurately and thus provide an alternative approach to study their relationship with protein structure and dynamics.[22−24] A number of DFT studies have been carried out for protein J coupling constants.[25−29] Case and Brüschweiler have derived a new set of Karplus equations for six ^{3}J-couplings involving the backbone torsional angle based on DFT calculations of the alanine dipeptide and found that they are generally in good agreement with Karplus equations from experimental values.[27] Unfortunately, the computational cost of quantum chemical calculation of J coupling constants is so expensive that these studies were limited to small peptide models, which also ignore hydrogen bonding, electrostatic, and substituent effects. Recently, we have developed an automated fragmentation quantum mechanics/molecular mechanics (AF-QM/MM) approach that incorporates all protein environmental effects in the calculation of local properties.[30] It was demonstrated that this approach is able to predict protein NMR chemical shifts accurately at the *ab initio* and DFT level. In this paper, we have extended this approach to compute vicinal J coupling constants for the 56-residue protein GB3. Bax and co-workers have measured three ϕ-dependent scalar coupling constants ($^3J(H^N,H^\alpha)$, $^3J(H^N,C^\beta)$, $^3J(H^N,C')$) for this protein with high precision experimental techniques and showed a remarkable improvement for all three ^{3}J-couplings when the Karplus parameters were fit to the NMR structure (PDB: 2OED) rather than the X-ray structure (PDB: 1IGD).[19] The backbone ϕ dihedral angles in the NMR and X-ray structures are quite close to each other with root-mean-square deviations (RMSDs) of 3.4°. However, the NMR structure is based on a very large number of residue dipolar couplings (RDCs) in five different alignment media and thus has accurate positions for H^N and H^α atoms relative to the protein backbone, while the hydrogen atoms were added into the X-ray structure under the assumptions of ideal tetrahedral geometry at C^α and idealized in-plane postions for H^N. They then took backbone dynamics into account by adding exponential functions into the Karplus parameters under the assumption of a Gaussian distribution for the backbone dihedral angle.[31] They found that internal backbone dynamics cannot explain all the discrepancies between experimental values and those from the Karplus equation, suggesting other effects, such as substituent, hydrogen bonding and local geometric distortions, have significant contributions to ^{3}J-coupling values.[18,19] Our AF-QM/MM approach is able to include these effects automatically during the calculation and thereby allows us to obtain a complete understanding of static and dynamic effects on J coupling constants. Moreover, we carried out the same calculations for another protein ubiquitin, which also has been extensively measured for backbone ^{3}J-coupling values, to test the transferability of Karplus equations.

METHODS

Quantum Mechanical Calculations of J Couplings. In our automated fragmentation approach, the entire protein is divided into nonoverlapping fragments termed core regions. The residues within a certain range from the core region are assigned as the buffer region. Both the core region and its buffer region are treated by quantum mechanics, while the remainder of the protein was described using an empirical point-charge model. The implementation details of the AF-QM/MM approach have been reported previously.[30,32−35] Here, we only describe the construction of the buffer region for J coupling constant calculation as opposed to NMR chemical shift calculations, which was described previously. Since J coupling constant calculations are relatively expensive, we want to keep the QM region as small as possible, while retaining as much "realism" as possible. Meanwhile, we also want to include all significant environmental effects in our J coupling constant calculations. The two neighboring residues around the core region are included in the buffer region. Any residue that forms a hydrogen bond with any atoms in the core residue is also included in the buffer region (see Figure 1). The remaining atoms in the protein are treated as point charges to account for long-range electrostatic interactions.

The quantum mechanical calculations of J coupling constants were performed at the PW91PW91[36,37]/IGLO-III[38] level using the Gaussian03 program.[39] According to the Ramsey theory,[40] there are four electronic mechanisms that contribute to J coupling constants, namely the Fermi contact (FC) term, the

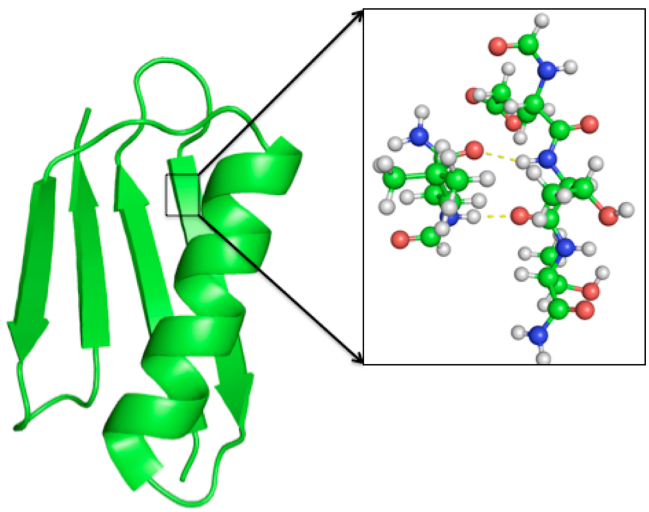

Figure 1. Structure of GB3 and a blow-up illustrating the subsetting scheme used in the AF-QM/MM approach for J coupling constant calculations.

dx.doi.org/10.1021/ct400631b | J. Chem. Theory Comput. 2013, 9, 4653−4659

diamagnetic spin−orbit (DSO) term, the paramagnetic spin−orbit (PSO) term, and the spin-dipole (SD) term. Although the FC term is usually dominant, it has been shown that the other three terms may still have nonnegligible contributions to J coupling constants.[41−43] Therefore, our calculcations included all four terms. The Perdew−Wang exchange and correlation functional has been demonstrated to reproduce experimental J coupling constants with good accuracy.[26,27] Since the dominated FC term involves the calculation of the electron density at the nuclei, it is imperative that basis sets of at least triple-ζ quality augmented with both diffuse and tight functions are used for J coupling calculations.[42] The IGLO-III basis set contains 11 s-type and 7 p-type Gaussian functions on the first row atoms along with two uncontracted polarization functions. Moreover, our theory level is consistent with that used in previous work carried out by Case and Brüschweiler.[27]

Molecular Dynamics Simulation. The NMR structure of GB3 (PDB: 2OED) was used as the starting point for the MD simulation using the AMBER ff99sb force field.[44] The protein was solvated in a truncated octahedral water box using the TIP3P[45] model with 8 Å between the edge of the box and the protein and minimized prior to the MD simulation. The SHAKE algorithm was employed to constrain X−H bonds to their equilibrium values.[46] The particle-mesh Ewald method was used to treat the long-range electrostatics interactions. The system was gradually heated from 0 to 300 K with decreasing weak constraints on the heavy atoms of the protein. During the last step of equilibration, the constraints were removed entirely, and the production simulations were performed at 300 K for 48 ns with a 2-fs time step. Constant temperature was maintained using the Berendsen coupling procedure.[47] Snapshots for subsequent analysis were taken every 2 ps. All simulations were carried out using PMEMD module from the AMBER suite of programs.[48] The generalized order parameter (S^2) was estimated by the plateau value of the autocorrelation function of the N−H vector:

$$C_i(t) = \langle P_2(\mu(\tau)\cdot\mu(\tau + t))\rangle \quad (2)$$

where μ is a unit vector pointing along the N−H bond and $P_2(x) = (3x^2 - 1)/2$ is the second Legendre polynomial. Prior to the analysis of the MD trajectories, the overall translation and rotation motions of the protein were removed so that the correlation function depended on the internal dynamics only. Three representative structures were generated by the standard pairwise RMSD cluster analysis over the entire 48 ns MD trajectory, as implemented in the PTRAJ module.

RESULTS AND DISCUSSION

GB3. *Static Effects.* As mentioned above, there are two very high-resolution structures available for GB3: 1IGD from X-ray crystallography (1.1 Å)[49] and 2OED from NMR spectroscopy.[50] These two structures are very close to each other with a backbone RMSD of 0.32 Å. However, 2OED has been refined on the basis of a very large number of RDCs recorded in five different media, allowing the amide N−H vector to bend out of the peptide plane. The original X-ray structure 1IGD does not have hydrogen atoms, and thus, they were added at idealized positions: a perfect tetrahedral geometry at C^α and the ideal in-plane position for H^N. The AF-QM/MM calculated J coupling constants based on 2OED have a much better agreement with the experimental values than those based on 1IGD (Figure 2): the RMSDs were 0.82 versus 1.18 Hz for $^3J(H^N,H^\alpha)$, 0.31 versus 0.51 Hz for $^3J(H^N,C^\beta)$, and 0.45 versus 0.55 Hz for $^3J(H^N,C')$. A noticeable example is Val21. The calculated values from 2OED and 1IGD are 4.7 and 6.5 Hz, respectively, with the former being much closer to the experimental value of 4.3 Hz. The backbone ϕ torsional angles for Val21 in 2OED and 1IGD are almost identical (−76.8°), whereas the H^N−N−C^α−H^α dihedral angles are quite different: −127.8° for 2OED and −141.3° for 1IGD. Bax and co-workers have found that the NMR structure of GB3 results in better fits to the Karplus equation than the X-ray structure.[19] Our calculations suggest that the hydrogen positions relative to the backbone atoms have a significant impact on the accuracy of calculated J coupling constants and that they can be accurately derived from a large number of RDCs in different media, as was done in the case of 2OED.

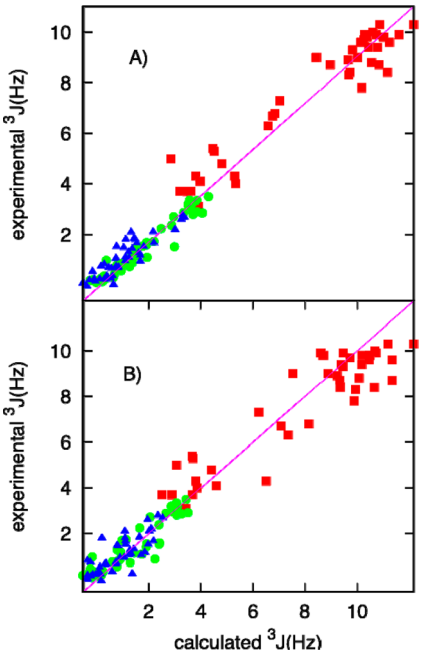

Figure 2. Comparison of the AF-QM/MM calculated $^3J(H^N,H^\alpha)$ (red), $^3J(H^N,C^\beta)$ (green), and $^3J(H^N,C')$ (blue) based on 2OED (A) and 1IGD (B) structures with experimental values. The RMSD of the three J coupling constants from 2OED are 0.82, 0.31, and 0.45 Hz, respectively, The RMSD of the three J coupling constants from 1IGD are 1.18, 0.51, and 0.55 Hz, respectively.

Figure 3 plots the calculated $^3J(H^N,H^\alpha)$ coupling constants for 2OED and 1IGD using our AF-QM/MM approach along with experimental values against the variation of dihedral angle ϕ. Three empirical Karplus curves are also included for comparison: two of them (GB3 and UBQ) are derived from experimental values based on GB3[13] and ubiquitin,[11] respectively, the last one (DFT1) is based on DFT calculations for an alanine peptide model from Case and Buschweiler's paper.[27] It is apparent that our calculated coupling values are strongly dependent on the intervening dihedral angle, confirming the general validity of the Karplus equation. However, both calculated and experimental values from a number of residues deviate from the Karplus curves significantly. These discrepancies can be caused by protein dynamics as discussed in the following section, and by static effects such as hydrogen bonding, substituent, and electrostatic effects (see Figure S1 of the Supporting Information). The hydrogen bonding effect is clearly illustrated by three consecutive threonine residues T16, T17, and T18 located in

dx.doi.org/10.1021/ct400631b | J. Chem. Theory Comput. 2013, 9, 4653−4659

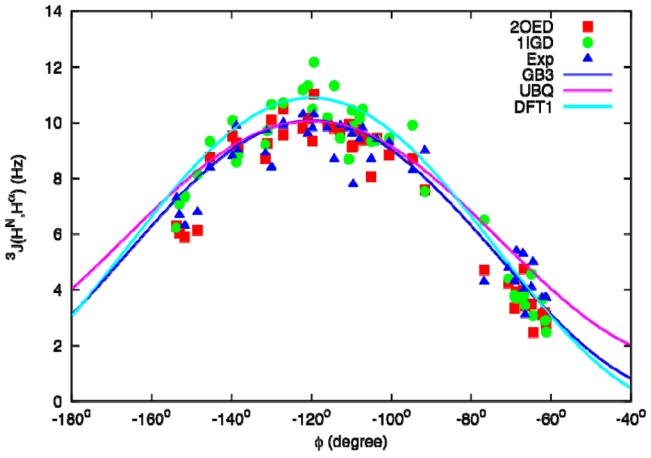

Figure 3. Plot of the calculated $^3J(H^N,H^\alpha)$ values from 2OED (red squares, AF-QM/MM) and 1IGD (green circles, AF-QM/MM) and the experimental values (blue triangles) against the backbone dihedral angle. Three Karplus curves are also included for comparison (θ = −60° in eq 1): the blue one is derived from GB3 data, the purple one is derived from ubiquitin data, and the cyan one is derived from the DFT calculations of an alanine model.

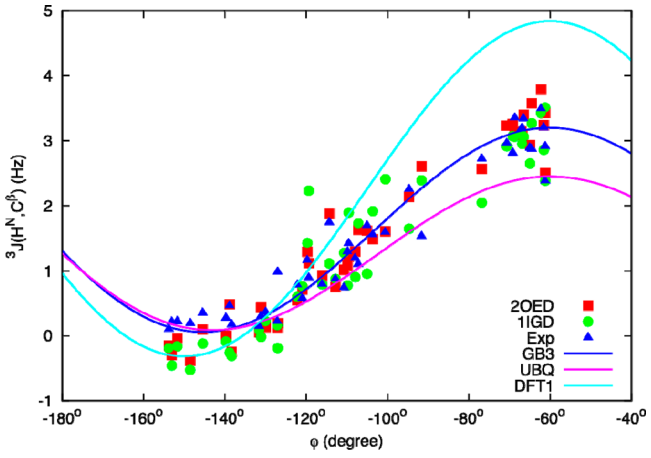

Figure 4. Plot of the calculated $^3J(H^N,C^\beta)$ values from 2OED (red squares, AF-QM/MM) and 1IGD (green circles, AF-QM/MM) and experimental values (blue triangle) against the backbone dihedral angle. Three Karplus curves are also included for comparison (θ = 60° in eq 1): the blue one is derived from GB3 data, the purple one is derived from ubiquitin data, and the cyan one is derived from the DFT calculations of an alanine model.

the β2 strand of GB3. Both T16 and T18 form double hydrogen bonds (with their amides as the donor and their carbonyl as the acceptor) with the residues in the β1 strand, causing their observed $^3J(H^N,H^\alpha)$ coupling constants to be 6 Hz. Whereas the observed value for T17 is 9 Hz because it does not form any hydrogen bond. It is difficult for the Karplus equation to catch these subtle differences through the fitting process since it has one-dimensional relationship with the dihedral angle ϕ. Our models include these hydrogen bonds explicitly in the QM region and thus successfully reproduce the experimental values. However, relatively large deviations were observed in an α-helical region (Ala23-Asp36), suggesting our model needs to be modified to better describe the electrostatic effects around these residues. As demonstrated by Zhu et al.,[33] a systematic investigation can be further carried out to examine the influence of cooperative hydrogen bonding effects, polarized protein-specific point charges and solvation models on calculated J coupling constants.

Figures 4 and 5 show the same plot for $^3J(H^N,C^\beta)$ and $^3J(H^N,C')$, respectively. These two J coupling constants have much smaller variations compared to $^3J(H^N,H^\alpha)$, and show the Karplus-type relationship with the backone ϕ torsional angle. The GB3 curve of $^3J(H^N,C^\beta)$ has the largest deviation from experimental values for Asp36. Our calculated values from both static structures have better agreement with experimental values because the QM region includes side chains in our AF-QM/MM approach. Moreover, an interesting feature of Figure 4 is that the Karplus curve based on the GB3 experimental values[19] deviates from that based on ubiquitin in the α-helical region (near ϕ = −60°), suggesting that the Karplus equation for $^3J(H^N,C^\beta)$ might have low transferability for residues in this region, which has also been pointed out by Vögeli et al.[13] The Karplus curve based on DFT calculations of the alanine model shows even larger discrepancy since it completely neglects substituent effects.[18,19] Figure 5 shows that the GB3 curve of $^3J(H^N,C')$ is almost identical with the UBQ curve. Val21 and Ala23 have relatively large differences between values obtained using Karplus curves and the experimental values. The AF-QM/MM results show improvement but still have significant deviations for these residues.

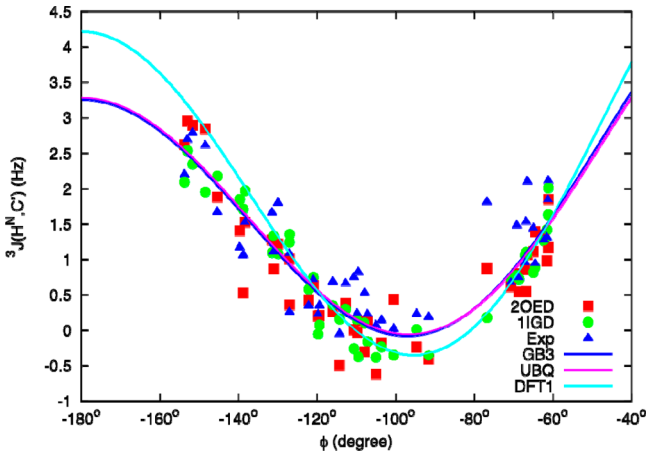

Figure 5. Plot of the calculated $^3J(H^N,C')$ values from 2OED (red squares, AF-QM/MM) and 1IGD (green circles, AF-QM/MM) and the experimental values (blue triangles) against the backbone dihedral angle. Three Karplus curves are also included for comparison (θ = 180° in eq 1): the blue one is derived from GB3 data, the purple one is derived from ubiquitin data, and the cyan one is derived from the DFT calculations of an alanine model.

Dynamic Effects. The overall RMSDs for all approaches are plotted in Figure 6A. The general picture is clear: the calculated values from 2OED are much more accurate than those from 1IGD, the Karplus curves based on the GB3 data are better than those based on the ubiquitin data set. The Karplus curve developed from DFT calculations on an alanine model is generally the worst. However, the accuracy of our calculated values based on 2OED is only comparable with that of the Karplus equation directly fitting the GB3 experimental data, although our AF-QM/MM approach captured all static effects on J coupling constants. Because any measured J coupling represents the time- and ensemble-average over fluctuations in protein structure, it is necessary to take protein dynamics into consideration when we compare calculated J coupling constants

dx.doi.org/10.1021/ct400631b | J. Chem. Theory Comput. 2013, 9, 4653−4659

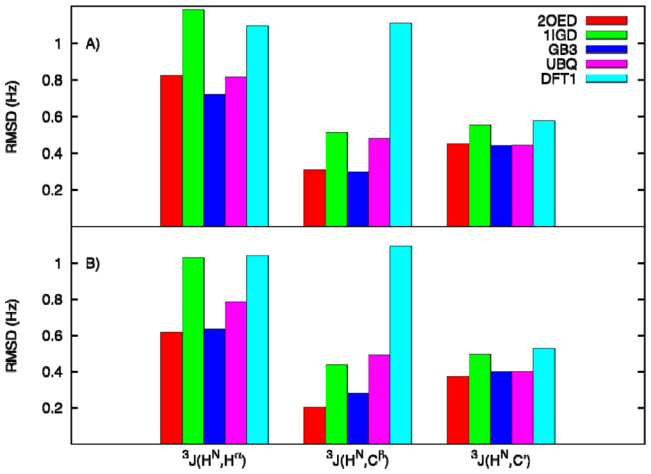

Figure 6. RMSDs of calculated $^3J(H^N,H^\alpha)$, $^3J(H^N,C^\beta)$, $^3J(H^N,C')$ from 2OED and 1IGD for all residues (A) and for those residues with the generalized order parameter (S^2) values larger than 0.8 (B). The RMSDs from three Karplus curves are also included for comparison. The color code is the same as that used in Figures 3−5.

directly with experiment. The N−H order parameters derived from the MD simulations of GB3 indicate that the two regions exhibiting the largest amplitude motions are located in the $\beta1-\beta2$ hairpin turn (residue 9−12) and in the loop connecting the α-helix to strand $\beta3$ (residue 37−41) (Figure 7A). These

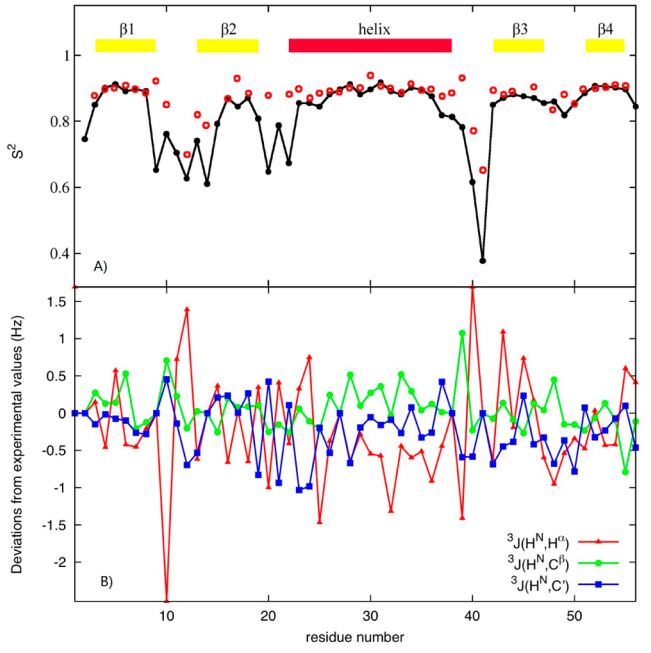

Figure 7. (A) Generalized order parameter S^2 from the MD simulations (black line) and the experimental data[53] (red circle). (B) Deviations of the computed $^3J(H^N,H^\alpha)$ (red), $^3J(H^N,C^\beta)$ (green), and $^3J(H^N,C')$ (blue) values (using the 2OED structure) from the experiment.

backbone motions have also been observed in NMR dipolar couplings[51] and ^{15}N heteronuclear relaxation studies.[52,53] The calculated J coupling constants for these mobile residues in 2OED show the largest deviation from experiment while those for the remaining residues display much smaller deviations (Figure 7B). If we exclude the data from the mobile residues for which the generalized order parameters are less than 0.8, the RMSDs of our calculated values from 2OED decrease dramatically and are more accurate than the Karplus equation based on the GB3 data, especially the RMSD of $^3J(H^N,C^\beta)$ (Figure 6B). The reductions of the RMSDs for the Karplus equations are quite small because they already absorb protein dynamics effects in an average way through the parametrization. Therefore, caution should be exercised when the Karplus equation is utilized to validate the accuracy of conformational populations generated by molecular mechanical force fields. Our AF-QM/MM approach will be able to extract accurate dynamical information from an ensemble of protein structures.

To further demonstrate this point, we have calculated J coupling constants for three representative structures from MD simulations and then averaged them based on their populations. The RMSDs between calculated values and experimental values for all non-Gly residues are plotted in Figure 8. The RMSDs of

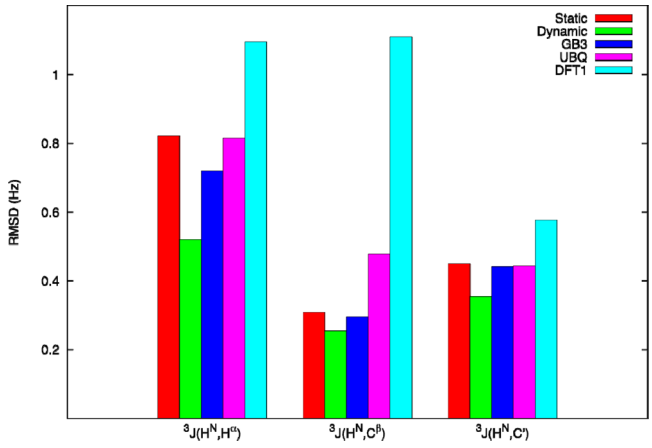

Figure 8. RMSDs of AF-QM/MM calculated $^3J(H^N,H^\alpha)$, $^3J(H^N,C^\beta)$, and $^3J(H^N,C')$ for all residues from one static structure (2OED) and from the average of three representative structures based on MD simulations. The RMSDs from three Karplus curves are also included for comparison (θ = −60°, 60° and 180° in eq 1, respectively, for $^3J(H^N,H^\alpha)$, $^3J(H^N,C^\beta)$, and $^3J(H^N,C')$ calculations).

Karplus equations are also included for comparison. After averaging the values from MD simulations, our AF-QM/MM approach yielded more accurate results compared to those based on one static structure (2OED). Most improvments come from the residues in the loop regions. Moreover, these results are significantly better than any Karplus curve, which is directly fitted to the experimental values.

Ubiquitin. We also performed the same set of calculations on two structures of the protein ubiquitin: 1UBQ is a 1.8 Å resolution X-ray structure[54] and 1D3Z is an NMR structure refined with RDC data.[55] The experimental values for all six vicinal J coupling are available although their precision is not as high as for those of GB3. Figure 9 shows the RMSDs for the calculated $^3J(H^N,H^\alpha)$, $^3J(H^N,C^\beta)$, and $^3J(H^N,C')$ values for those residues with S^2 values larger than 0.8, along with those from three Karplus equations. Again, our calculated values based on 1D3Z are superior to the Karplus equation results. The RMSD differences between the Karplus curve derived from the GB3 data set and that from ubiquitin highlight the transferability problem of the Karplus equation. Figure 10 is the same plot for $^3J(C',H^\alpha)$, $^3J(C',C^\beta)$, and $^3J(C',C')$. Interestingly, for $^3J(C',C^\beta)$, and $^3J(C',C')$ whose spins do not involve the backbone hydrogen atoms, the calculated values from the NMR

dx.doi.org/10.1021/ct400631b | J. Chem. Theory Comput. 2013, 9, 4653−4659

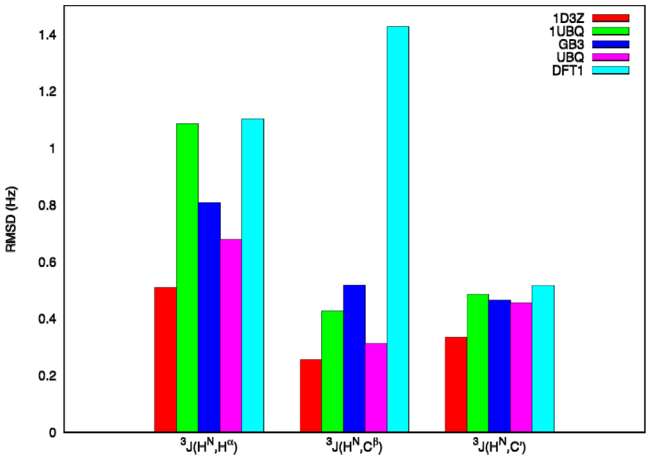

Figure 9. RMSDs of AF-QM/MM calculated $^3J(H^N,H^\alpha)$, $^3J(H^N,C^\beta)$, and $^3J(H^N,C')$ from 1D3Z and 1UBQ for those residues with the generalized order parameter (S^2) values larger than 0.8. The RMSDs from three Karplus curves are also included for comparison.

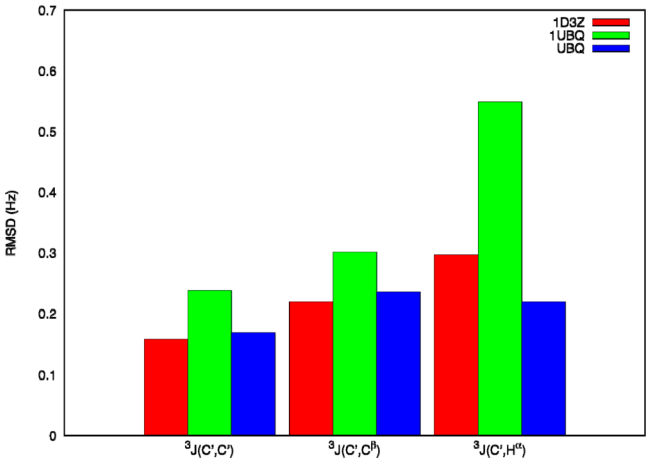

Figure 10. RMSDs of AF-QM/MM calculated $^3J(C',H^\alpha)$, $^3J(C',C^\beta)$, and $^3J(C',C')$ from 1D3Z and 1UBQ for those residues with the generalized order parameter (S^2) values larger than 0.8.

structure are still slightly better than those from the X-ray structure.

CONCLUSIONS

Recent experimental developments have yielded very accurate measurements for J coupling constants for proteins, which provide unique insights into the structure and dynamics of the protein under study. One study has showed that the discrepancy between experimental coupling constants and the Karplus equation cannot be assigned as a dynamical effect only, suggesting that other static effects, such as hydrogen bonding, substituent effects, and small geometrical distortations caused by local strain, might play an important role. Our AF-QM/MM approach includes these effects naturally and thus provides an efficeint tool to understand the multidimensional relationship between J coupling constants and protein structure and dynamics. Indeed, our calculated $^3J(H^N,H^\alpha)$, $^3J(H^N,C^\beta)$, and $^3J(H^N,C')$ values for GB3 using this approach yield better agreement with experimental values than the available Karplus equations after taking dynamical effects into account. The large improvement in the accuracy of the calculated values based on the NMR structure relative to the X-ray structure underscores the importance of the knowledge of the positioning of hydrogen atoms relative to the backbone atoms.[19] The excellent agreement of our results for these vicinal J coupling constants suggests that extension of this study to other J couplings that might not follow the Karplus equation would be fruitful. Overall, the combination of highly accurate experimental data with our AF-QM/MM approach is able to enhance the power of J coupling constants to probe the structure and dynamics of proteins and other biomolecules.

ASSOCIATED CONTENT

Supporting Information

Figures S1 shows the AF-QM/MM calculated $^3J(H^N,C')$,$^3J(H^N,H^\alpha)$, and $^3J(H^N,C^\beta)$ values for ASP40 of GB3 at the B3LYP/6-31G** level as a function of the size of the buffer region. This material is available free of charge via the Internet at http://pubs.acs.org.

AUTHOR INFORMATION

Corresponding Authors

*E-mail: xiaohe@phy.ecnu.edu.cn.
*E-mail: merz@qtp.ufl.edu.

Notes

The authors declare no competing financial interest.

ACKNOWLEDGMENTS

B. Wang and K. M. Merz thank the National Science Foundation (NSF) of the United States (MCB-0517055), and X. He acknowledges the National Natural Science Foundation of China (Grant No. 21303057) for financial support of this research. Computing support from the University of Florida High Performance Computing Center is also gratefully acknowledged.

REFERENCES

(1) Karplus, M. *J. Chem. Phys.* **1959**, *30*, 11.
(2) Karplus, M. *J. Am. Chem. Soc.* **1963**, *85*, 2870.
(3) Case, D. A.; Dyson, H. J.; Wright, P. E. *Methods Enzymol.* **1994**, *239*, 392.
(4) Barfield, M.; Chakrabarti, B. *Chem Rev* **1969**, *69*, 757.
(5) Bax, A.; Grzesiek, S. *Acc. Chem. Res.* **1993**, *26*, 131.
(6) Contreras, R. H.; Peralta, J. E. *Prog. Nucl. Magn. Reson. Spectrosc.* **2000**, *37*, 321.
(7) Wishart, D. S.; Sykes, B. D.; Richards, F. M. *J. Mol. Biol.* **1991**, *222*, 311.
(8) Altona, C.; Sundaralingam, M. *J. Am. Chem. Soc.* **1973**, *95*, 2333.
(9) Pardi, A.; Billeter, M.; Wuthrich, K. *J. Mol. Biol.* **1984**, *180*, 741.
(10) Hu, J. S.; Bax, A. *J. Am. Chem. Soc.* **1996**, *118*, 8170.
(11) Wang, A. C.; Bax, A. *J. Am. Chem. Soc.* **1996**, *118*, 2483.
(12) Hu, J. S.; Bax, A. *J. Am. Chem. Soc.* **1997**, *119*, 6360.
(13) Schmidt, J. M.; Blumel, M.; Lohr, F.; Ruterjans, H. *J. Biomol. NMR* **1999**, *14*, 1.
(14) Case, D. A. *Curr Opin Struc Biol* **2000**, *10*, 197.
(15) Graf, J.; Nguyen, P. H.; Stock, G.; Schwalbe, H. *J. Am. Chem. Soc.* **2007**, *129*, 1179.
(16) Best, R. B.; Buchete, N. V.; Hummer, G. *Biophys. J.* **2008**, *95*, L7.
(17) Wickstrom, L.; Okur, A.; Simmerling, C. *Biophys. J.* **2009**, *97*, 853.
(18) Haasnoot, C.; de Leeuw, F.; Altona, C. *Tetrahedron* **1980**, *36*, 2783.
(19) Vögeli, B.; Ying, J. F.; Grishaev, A.; Bax, A. *J. Am. Chem. Soc.* **2007**, *129*, 9377.
(20) Headgordon, T.; Headgordon, M.; Frisch, M. J.; Brooks, C. L.; Pople, J. A. *J. Am. Chem. Soc.* **1991**, *113*, 5989.

(21) Edison, A. S.; Weinhold, F.; Westler, W. M.; Markley, J. L. *J. Biomol. NMR* **1994**, *4*, 543.
(22) Malkin, V. G.; Malkina, O. L.; Casida, M. E.; Salahub, D. R. *J. Am. Chem. Soc.* **1994**, *116*, 5898.
(23) Helgaker, T.; Watson, M.; Handy, N. C. *J. Chem. Phys.* **2000**, *113*, 9402.
(24) Sychrovsky, V.; Grafenstein, J.; Cremer, D. *J. Chem. Phys.* **2000**, *113*, 3530.
(25) Dingley, A. J.; Masse, J. E.; Peterson, R. D.; Barfield, M.; Feigon, J.; Grzesiek, S. *J. Am. Chem. Soc.* **1999**, *121*, 6019.
(26) Scheurer, C.; Brüschweiler, R. *J. Am. Chem. Soc.* **1999**, *121*, 8661.
(27) Case, D. A.; Scheurer, C.; Brüschweiler, R. *J. Am. Chem. Soc.* **2000**, *122*, 10390.
(28) Cornilescu, G.; Bax, A.; Case, D. A. *J. Am. Chem. Soc.* **2000**, *122*, 2168.
(29) Chou, J. J.; Case, D. A.; Bax, A. *J. Am. Chem. Soc.* **2003**, *125*, 8959.
(30) He, X.; Wang, B.; Merz, K. M., Jr. *J. Phys. Chem. B* **2009**, *113*, 10380.
(31) Brüschweiler, R.; Case, D. A. *J. Am. Chem. Soc.* **1994**, *116*, 11199.
(32) Zhu, T.; He, X.; Zhang, J. Z. H. *Phys. Chem. Chem. Phys.* **2012**, *14*, 7837.
(33) Zhu, T.; Zhang, J. Z. H.; He, X. *J. Chem. Theory Comput.* **2013**, *9*, 2104.
(34) Tang, S. S.; Case, D. A. *J. Biomol. NMR* **2011**, *51*, 303.
(35) Case, D. A. *Curr. Opin. Struct. Biol.* **2013**, *23*, 172.
(36) Perdew, J. P. *Phys. Rev. B* **1986**, *33*, 8822.
(37) Perdew, J. P.; Yue, W. *Phys. Rev. B* **1986**, *33*, 8800.
(38) Kutzelnigg, W.; Fleischer, U.; Schinder, M. In *NMR, Basic Principles and Progress*; Diehl, P., Fluck, E., Gnther, H., Kosfeld, R., Seelig, J., Eds.; Spinger: Berlin, 1990; Vol. *23*, p 167.
(39) Frisch, M. J.; Trucks, G. W.; Schlegel, H. B.; Scuseria, G. E.; Robb, M. A.; Cheeseman, J. R.; Montgomery, J. A. J.; Vreven, T.; Kudin, K. N.; Burant, J. C.; Millam, J. M.; Iyengar, S. S.; Tomasi, J.; Barone, V.; Mennucci, B.; Cossi, M.; Scalmani, G.; Rega, N.; Petersson, G. A.; Nakatsuji, H.; Hada, M.; Ehara, M.; Toyota, K.; Fukuda, R.; Hasegawa, J.; Ishida, M.; Nakajima, T.; Honda, Y.; Kitao, O.; Nakai, H.; Klene, M.; Li, X.; Knox, J. E.; Hratchian, H. P.; Cross, J. B.; Bakken, V.; Adamao, C.; Jaramillo, J.; Gomperts, R.; Stratmann, R. E.; Yazyev, O.; Austin, A. J.; Cammi, R.; Pomelli, C.; Ochterski, J. W.; Ayala, P. Y.; Morokuma, K.; Voth, G. A.; Salvador, P.; Dannenberg, J. J.; Zakrzewski, V. G.; Dapprich, S.; Daniels, A. D.; Strain, M. C.; Farkas, O.; Malick, D. K.; Rabuck, A. D.; Raghavachari, K.; Foresman, J. B.; Ortiz, J. V.; Cui, Q.; Baboul, A. G.; Clifford, S.; Cioslowski, J.; Stefanov, B. B.; Liu, G.; Liashenko, A.; Piskorz, P.; Komaromi, I.; Martin, R. L.; Fox, D. J.; Keith, T.; Al-Laham, M. A.; Peng, C. Y.; Nanayakkara, A.; Challacombe, M.; Gill, P. M. W.; Johnson, B.; Chen, W.; Wong, M. W.; Gonzalez, C.; Pople, J. *Gaussian03* C.02; Gaussian, Inc.: Wallingford, CT, 2004.
(40) Ramsey, N. F. *Phys. Rev.* **1953**, *91*, 303.
(41) Helgaker, T.; Jaszuński, M.; Ruud, K. *Chem. Rev.* **1999**, *99*, 293.
(42) Jensen, F. *J. Chem. Theory Comput* **2006**, *2*, 1360.
(43) Maximoff, S. N.; Peralta, J. E.; Barone, V.; Scuseria, G. E. *J. Chem. Theory Comput.* **2005**, *1*, 541.
(44) Hornak, V.; Abel, R.; Okur, A.; Strockbine, B.; Roitberg, A.; Simmerling, C. *Proteins* **2006**, *65*, 712.
(45) Jorgensen, W. L.; Chandrasekhar, J.; Madura, J. D.; Impey, R. W.; Klein, M. L. *J. Chem. Phys.* **1983**, *79*, 926.
(46) Allen, M. P.; Tildesley, D. J. *Computer Simulations of Liquids*; Clarendon Press: Oxford, 1987.
(47) Berendsen, H. J. C.; Postma, J. P. M.; Vangunsteren, W. F.; Dinola, A.; Haak, J. R. *J. Chem. Phys.* **1984**, *81*, 3684.
(48) Case, D. A.; Cheatham, T. E., III; Darden, T.; Gohlke, H.; Luo, R.; Merz, K. M., Jr.; Onufriev, A.; Simmerling, C.; Wang, B.; Woods, R. J. *J. Comput. Chem.* **2005**, *26*, 1668.
(49) Derrick, J. P.; Wigley, D. B. *J. Mol. Biol.* **1994**, *243*, 906.
(50) Ulmer, T. S.; Ramirez, B. E.; Delaglio, F.; Bax, A. *J. Am. Chem. Soc.* **2003**, *125*, 9179.
(51) Clore, G. M.; Schwieters, C. D. *Biochemistry* **2004**, *43*, 10678.
(52) Hall, J. B.; Fushman, D. *J. Biomol. NMR* **2003**, *27*, 261.
(53) Yao, L. S.; Grishaev, A.; Cornilescu, G.; Bax, A. *J. Am. Chem. Soc.* **2010**, *132*, 4295.
(54) Vijaykumar, S.; Bugg, C. E.; Cook, W. J. *J. Mol. Biol.* **1987**, *194*, 531.
(55) Cornilescu, G.; Marquardt, J. L.; Ottiger, M.; Bax, A. *J. Am. Chem. Soc.* **1998**, *120*, 6836.